Dynamics and Model Research on the Electrosorption by Activated Carbon Fiber Electrodes

Lan Ma [1,2], **Luyue Huang** [1,2], **Yongyi Xu** [3], **Chang Liu** [1,2], **Feng Wang** [3], **Haoruo Xing** [1,2] and **Shuangchen Ma** [1,2,*]

[1] Hebei Key Lab of Power Plant Flue Gas Multi-Pollutants Control, Department of Environmental Science and Engineering, North China Electric Power University, Baoding 071003, China; 18632263983@163.com (L.M.); huangluyue19971103@163.com (L.H.); liuchang0932@126.com (C.L.); xhr623@163.com (H.X.)

[2] MOE Key Laboratory of Resources and Environmental Systems Optimization, Beijing 102206, China

[3] China Power Hua Chuang Electricity Technology Research Company Ltd., Suzhou 215123, China; yyxu@cpibj.com.cn (Y.X.); wangfeng@cpibj.com.cn (F.W.)

* Correspondence: msc1225@163.com; Tel.: +86-139-302-376-90

Abstract: Electrosorption is a new emerging technology for micro-polluted water treatment. To gain a more accurate understanding of the mass and charge transfer process of electrosorption, the electrosorption performance of activated carbon fiber (ACF) electrodes with various concentrations was studied. In this paper, quasi-first-order and quasi-second-order dynamic equations, and an intra-particle diffusion equation were used to describe the electrosorption behaviors. It is believed that the electrosorption process is dominated by physical adsorption for ACF material, and the most important rate control steps in this process are intra-diffusion and electromigration steps. Based on the experimental results and modified Donnan model theory, a considerable electrosorption dynamic model which considered the influence of physical adsorption and the intra-diffusion resistance was proposed. This model quantitatively described the salt adsorption and charge storage in the ACF electrode and can fit the experimental data well.

1. Introduction

Water is an indispensable resource for the development of human society. Although most of the Earth's surface is covered by water, due to technical and economic reasons, the freshwater that can be used by humans only accounts for 0.26% of the Earth's total water, and only 0.007% of the total water can be directly used by humans [1]. Nowadays, water shortage has been listed as an issue of global importance. Therefore, to ensure the sustainable development of water resources, the strengthening of water pollution control, and wastewater reuse, efforts have been made to improve water supply and reuse purification processes [2].

The traditional desalination methods currently used have certain drawbacks in the implementation process. For example, the traditional distillation method has slow evaporation speed, low water production efficiency, and high energy consumption [3]. Although ion exchange (IE) has high water production efficiency, a large amount of acid and alkali is required for resin regeneration, and secondary pollution is likely to occur, which limits its further industrial application in the field of high-concentration brine desalination [4]. The electrodialysis (ED) treatment method [5] and reverse osmosis (RO) desalination [6] have issues in membrane fouling, maintenance and complex pretreatment. With the continuous advancement of science and technology, new water treatment processes have been emerging. In recent decades, electrosorption technology (also called capacitive deionization, CDI) has attracted widespread attention from experts and scholars due to its low energy consumption, high water production efficiency, and no secondary pollution [7].

Electrosorption is defined as the potential-induced adsorption of ions onto the surface of charged electrodes. When a lower voltage (about 1–1.5v) is applied to the solution at

which no electrolysis reactions occur [8], the interface between the electrode plate and the solution forms an electric double-layer structure with a certain adsorption capacity. This electric double-layer can attract positive/negative ions in the water to move to the cathode/anode and hold in the structure of the electrode surface, pores, and electric double layer [9]. The purpose of separating the electrolyte and solution is thus achieved. With the progress of the desalination process, due to the limited capacity of the electric double layer, the saturated adsorption capacity is gradually reached. At this time, the desalination process reaches a macroscopic equilibrium state; that is, the adsorption rate and the desorption rate are equal. Once the external power supply is removed or the power supply's polarity is reversed, the charged ions enriched on the cathode and anode plates are quickly released under the effect of the electrostatic force and the tangential force of the water flow [10]. This process can realize the recovery of the adsorption capacity of the electrode plate in a short time, and the electric adsorption device can be reused. Figure 1a is a schematic diagram of the desalination process; Figure 1b is a schematic diagram of the regeneration process.
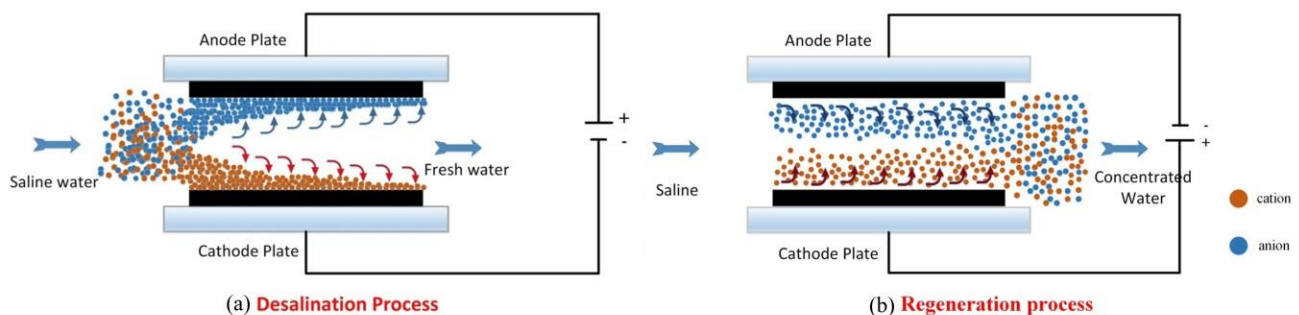
Figure 1. Electrosorption desalination (**a**) and the regeneration process (**b**) diagram.

The innovation of porous materials has always been a research hotspot in the related fields. However, considering practical factors such as economy and complexity of the manufacturing process, activated carbon fiber is currently an industrially competitive electrode material by virtue of its rich raw material, a low price and a large specific surface area. In this study, the concept of the electric double layer (EDL) and electrosorption dynamics were used to understand salt adsorption and charge storage in the micropores. An electrosorption dynamic model considered the overlap effect of the EDL and the intra-diffusion resistance was proposed to quantitatively describe the electrosorption behaviors of activated carbon fiber (ACF) electrodes.

Through rapid development in recent decades, this technology has been applied to sea water desalination, wastewater recovery, water softening, and other water treatment fields.

2. Classic Electric Double Layer Models and m-D Model

2.1. Classic Electric Double Layer Models

Classic electric double-layer models contain three forms: the Helmholtz–Perrin model (HP model) [11], Gouy–Chapman model (GC model) [12] and the Gouy–Chapman–Stern model (GCS model) [13]. Figure 2 shows the structure of these models and Table 1 summarizes the characteristic equation as well as the scope of the application of these classic EDL models.
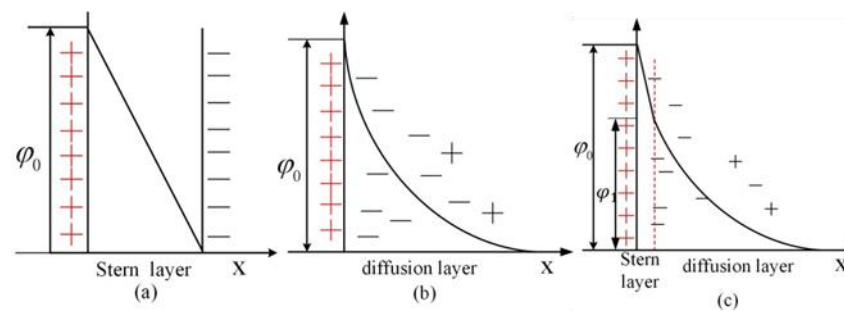
Figure 2. Structural of classic electric double layer (EDL) models. From left to right are the Helmholtz–Perrin (**a**) Gouy–Chapman model (**b**) and the Gouy–Chapman–Stern models (**c**), respectively.

Table 1. Main mechanisms and the scope of application of the three classic interface models.

EDL Model	Characteristic Equation	Scope of Application
Helmholtz–Perrin model	$\varphi_0 = \sigma\delta/\varepsilon$	Suitable for the EDL structure with small total surface charge q or high electrolyte concentration.
Gouy–Chapman model	$\varphi_x = \varphi_0 e^{-Kx}$	Suitable for low concentration electrolytes, but not accurate enough.
Gouy–Chapman–Stern model	$\sigma = \sqrt{8cRT\varepsilon_0\varepsilon}\sinh\frac{|Z|\varphi_1 F}{2RT}$	Suitable for situations where there is no special adsorption.

In these characteristic equations, K represents the Debye–Hueckel constant; k represents the Boltzmann constant; Z represents the number of charges carried by the ions; ε represents the relative permittivity; ε_0 represents the vacuum permittivity; F represents the Faraday constant; φ_0 is the solid surface potential; φ_1 is the diffusion potential difference; φ_x is the electric potential in the x direction; σ is the surface charge density of the electrode; and c represents the solution concentration.

The GCS model solves the deficiencies of the Helmholtz–Perrin and the Gouy–Chapman models, simultaneously considering the effects of ion thermal motion and electrostatic gravity. However, it is not enough to only consider the electrostatic force as a driving force for mass transfer because special adsorption also plays an important role in electrosorption. Most inorganic cations do not undergo special adsorption. Except for fluoride ion, special adsorption occurs for almost all inorganic anions. With or without special adsorption, the Stern layer's structures are different [14].
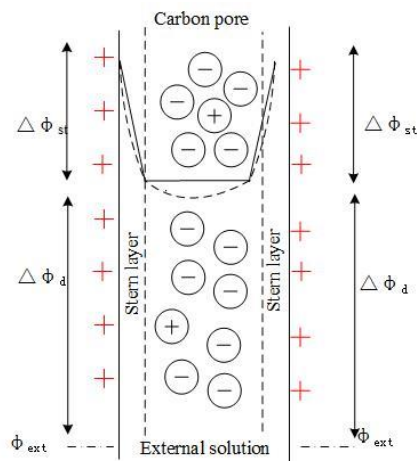
2.2. Modified Donnan Model

The thickness of the diffusion layer determined by the solution concentration, voltage, and the size of the adsorbed ion. In the GCS model assumptions, the voltage of the diffusion layer decreases exponentially and tends to zero as the distance from the electrode surface increases. However, in reality, if the diameter of the pore size is large enough, the electrode potential at the intermediate plane of the pore is zero, and the two electric double layers do not overlap or interfere with each other. As the diameter of the pore size decreases, the electric double layers with the same charge will gradually overlap, so the potential of the intermediate plane increases. Therefore, the ions that enter the pore channel are repelled by the electric potential generated by the strongly overlapped electric double layer, so the resistance of ions entering the channel increases [15], which is called the intra-diffusion resistance.

When the pore size is reduced to the cut-off pore size, and the potential distribution in the electric double layer tends to be stable, that is, the surface charge density is 0, counter ions cannot enter the pores and the capacitance effect is weakened.

To solve the above practical problem, Porada et al. proposed a modified Donnan model (m-D model) [16]. This model considers that the storage of salt occurs in the pore

volume, which is less than 2 nm, rather than taking place along the pore surface (as assumed by the model established by Helmholtz or the GCS electric double-layer structure model). In Figure 3, the diagram of the modified Donnan model was shown.

Figure 3. Diagram of the modified Donnan model.

In the m-D model, the electric double layer in the microporous area is considered to be strongly overlapping. Therefore, the electric potential in the micropores that are smaller than 2 nm does not vary with the position, and the electric potential in the micropores can be considered constant.

The modified Donnan model makes two corrections. The first point is to modify the Stern layer. Ions cannot approach the electrode surface indefinitely. This is because ions have a certain size and cannot approach a surface smaller than their radius. That is, between the electrode material and the solvated ions in the electrolyte, there is a Stern layer with no charge. The second correction is to include the chemical adsorption energy [17], which is represented by μ_{att}. The latter extension captures the effect that functional groups on the electrode surface can interact with ions to form chemical bonds, which is called fake adsorption capacity [18]. The following equation contains the above two corrections. This equation expresses the relationship between the salt concentration in the macropores of the electrode material and the salt concentration in the micropores:

$$c_{j,mi} = c_{j,mA} \times \exp\left(-Z_j \times \Delta\phi_d + \mu_{att}\right) \qquad (1)$$

In the equation, Z_j is the ion valence, for cations $Z_j = +1$, for anions $Z_j = -1$; $\Delta\phi_d$ is the Donnan potential difference formed between the micropores and the macropores. It is also the potential difference between the inside and outside of the carbon particles.

3. Experimental and Analysis of Electrosorption Dynamics

In order to model ion uptake into EDLs, the transport model must couple to an EDL structure model, which can relate the local potential drop across the EDL in the porous carbon particles, or at any pore walls, to the local ion flux into the EDL. Thus, obtaining accurate electrosorption model results depends on the use of an accurate EDL structure model. Therefore, it is necessary for us to carry out experiments to determine which electric double layer model is more suitable for the ACF electrodes, and what corrections need to be made to the model formula.

3.1. Characteristics of ACF Electrodes

The specific surface area of ACF was measured using an Autosorb-iQ2-MP type surface area analyzer. Figure 4a is the N_2 adsorption isotherm of the ACF. According to the International Union of Theoretical and Applied Chemistry (IUPAC) classification standards, the adsorption type of this material is type I. According to the characterization results,

the material's specific surface area is 1381.497 m^2/g, the micropore volume is 0.507 cm^3/g, the micro-pore surface area is 1293 m^2/g and the remaining surface area is 88.194 m^2/g. Figure 4b is the pore size distribution. The curve shows the rate of change of the pore volume with the diameter in different diameter ranges. The larger the value of the ordinate, the greater the number of holes in the diameter range. As can be seen from Figure 4b, the pore diameter of the ACF is mainly concentrated in two regions over the entire range, at about 1 and 2 nm. This means that the material belongs to a micro-porous material.
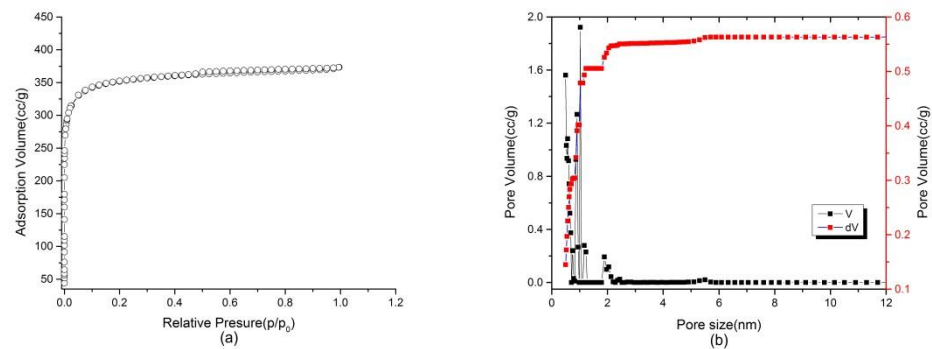

Figure 4. (**a**) N$_2$ adsorption–desorption isotherms of activated carbon fiber (ACF); and (**b**) ACF's pore size distribution curve.

3.2. CDI System

Adsorption experiments were carried out in a flow-between system depicted in Figure 5. The system consisted of a recycling tank, a peristaltic pump, a custom-made module, a conductivity pen, and a DC power. The core of the CDI system was a custom-made module, which was a sandwich structure with a pair of electrodes. The size of the selected electrode material (activated carbon fiber) was 200 × 500 mm. The internal structure of the membrane pile is shown in Figure 6. The internal membrane stack components were fixed by the Plexiglas end plates, while providing external ports for fluid flow. A 1 mm thick rubber pad for sealing; a rubber ring to fix the ACF electrode, while sealing the electrode plate; a 316 L stainless steel plate was used as a current collector; and ACF was an adsorption carrier for anions and cations in solution. An insulating membrane (polyethylene fiber mesh) was placed in the middle position to provide a passage for fluid flow.
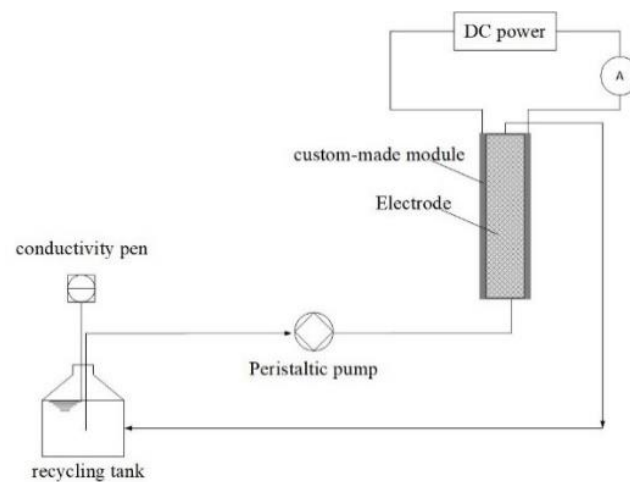
Figure 5. Schematic diagram of the electrosorption experiments.
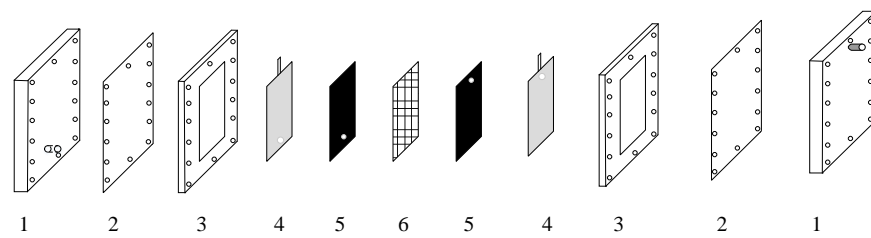
Figure 6. Schematic diagram of the inner structure of the capacitive deionization (CDI) module.

3.3. Experimental Method

In this experiment, a batch-mode method was used. The feed solution containing electrolytes was pumped from the recycling tank, passed through the module where ion electrosorption took place, and then flowed back to the recycling tank. The number of moles of salt in this method was constant. The difference in salinity between the initial and final situation could be multiplied by the total water volume in the whole system to calculate the number of ions removed from the water.

Experiments were conducted to investigate the effect of different initial concentrations on ion electrosorption and transport properties in CDI. There were five different concentrations of NaCl solution prepared for these experiments: 100, 300, 500, 800, and 1000 mg/L. Prior to each experiment, the whole system was flushed to a baseline salinity of less than 10 µs/cm using deionized water in single-pass mode. In this process, the external power supply's polarity was reversed, and the voltage was set to 0.8 V. This was the desorption step. Then, the electrosorption experiments began with the power supply of the CDI system and the pump being turned on simultaneously and ended when the adsorption equilibrium was reached. At this point, the adsorption step was over. In the adsorption step, the conductivity and current values were recorded every 60 s. Duplicate runs were carried out for each set of experimental conditions, and the average value was plotted. The volume of the initial solution for each experiment was 500 mL. The charging voltage between the two carbon electrodes was set to $V_{cell} = 1.2$ V during the adsorption step, and the flow rate of the peristaltic pump was 40 mL/min. The purpose of this experiment was to clarify whether the electrosorption process is mainly physical adsorption or chemical adsorption or these two mechanisms occur simultaneously. When ACF was used as an electrode material, the internal diffusion process was a key step to control the electrosorption rate. All this work was preparation for the establishment of a CDI dynamic model.

3.4. Analysis and Discussion of Electrosorption Dynamics

Three model equations including quasi-first-order, quasi-second-order and intra-particle diffusion equation were employed to fit experimental data. Through the analysis of electrosorption dynamics, the more comprehensive understanding of electrosorption mass transfer resistance were beneficial to set up a more accurate dynamic model.

The forms of these equations can be formulated as

$$q = q_e\left(1 - e^{-k_1 t}\right) \tag{2}$$

$$q(1 + q_e k_2 t) = q_e^2 k_2 t \tag{3}$$

$$q = K_3 t^{0.5} + C \tag{4}$$

where q is the adsorption capacity per unit mass of adsorbent at any time t, mg/g; q_e is the adsorption capacity per unit mass of adsorbent when saturated adsorption is reached, mg/g; k_1 is the quasi-first-order dynamic adsorption constant, h^{-1}; k_2 is quasi-second-order dynamic adsorption constant, h^{-1}; K_3 is the intra-particle diffusion rate constant, mg/(g·min$^{1/2}$); C is the constant, mg/g; and t is adsorption time. For the quasi-first-order dynamic equation (Equation (2)) and quasi-second-order dynamic equation (Equation (3)),

the unit is the hour, but for the intra-particle diffusion equation (Equation (4)), the unit is the minute.

The results are shown in Figure 7, where the fitting curves of quasi-first-order and quasi-second-order dynamic equations are represented by the black solid line and the red dashed line, respectively. The fitting curves of the intra-diffusion equation are shown in Figure 8. The results of the whole fitting parameters are listed in Table 2. It can be seen from Figure 6 and Table 2 that the quasi-first-order dynamic equation can fit the experimental data better than the quasi-second-order dynamic equation due to the higher value of the correlation coefficient (R^2). These results suggested that the process of electrosorption follows the physical adsorption process of electric double-layer capacitors, and there is almost no Redox reaction. It is clearly indicated that when the initial concentration increased from 100 to 1000 mg/L, the quasi-first-order dynamic adsorption rate constants were gradually increased. There are two reasons for the explanation of this phenomenon [19]. One is that the concentration gradient between the bulk solution and the solid–liquid interface was increased, which promotes the rate of ion migration to the solid–liquid interface; the second is that the higher concentration enhances the surface charge density of the ACF electrode, so under the combined function of the driving force of the concentration gradient and the electrostatic, the electrosorption rate is significantly increased. From the figure above, we can also see that the equilibrium adsorption capacity has increased significantly. This phenomenon caused by the increase in ion concentration reduces the cut-off pore size of the ACF material. This reduction makes the micropores that are not used in the dilute solution also adsorb some ions, which improves the adsorption capacity and weakens the overlap effect of the electric double layer.
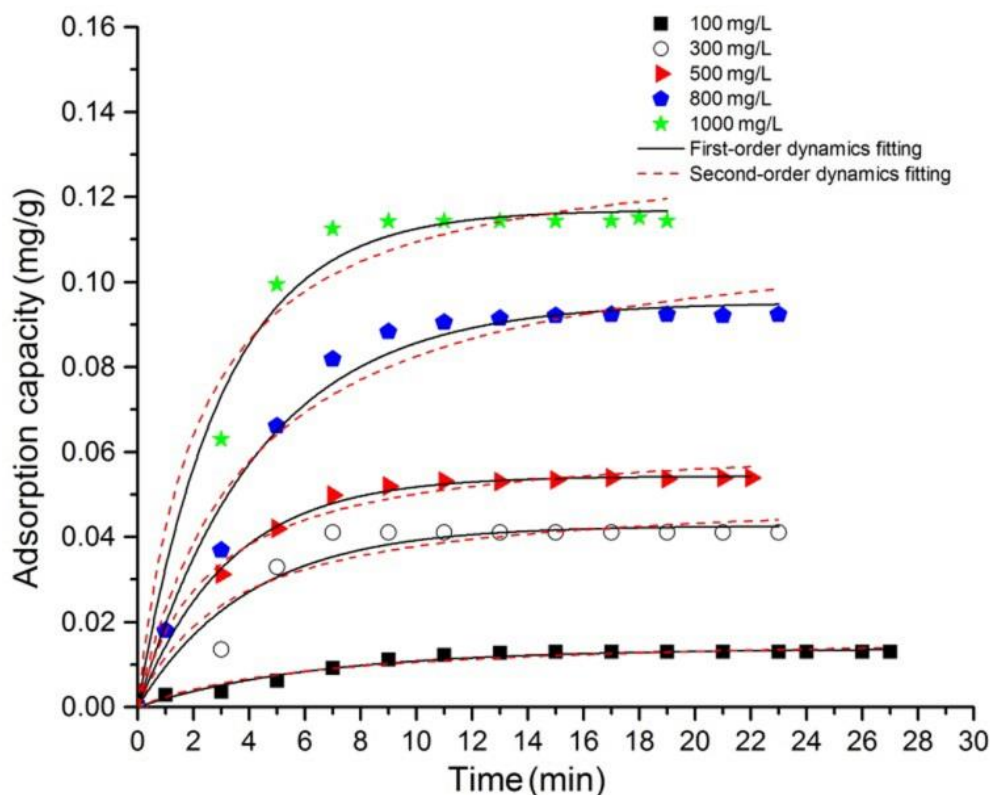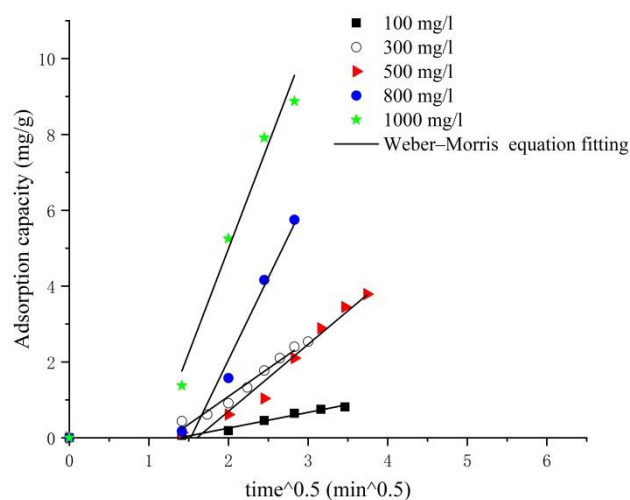

Figure 7. The curve of the electrosorption capacity with time under different concentrations.

Figure 8. The curve of the electrosorption capacity with time to the power of 0.5 under different concentrations.

Table 2. Dynamic equation fitting results.

Concentration (mg/L)	Quasi-First-Order			Quasi-Second-Order			Weber–Morris	
	q_e	k_1	R^2	q_e	k_2	R^2	k_3	R^2
100	0.01366	0.15724	0.97018	0.01719	9.24178	0.99423	0.4135	0.97552
300	0.04262	0.25256	0.92512	0.0504	5.96585	0.8875	1.4689	0.96226
500	0.05432	0.30579	0.99654	0.06329	6.00808	0.98454	1.7645	0.95526
800	0.09525	0.22942	0.98274	0.11552	2.16278	0.96123	4.3264	0.95935
1000	0.11693	0.3277	0.98165	0.13328	3.44591	0.95868	5.5119	0.9723

The intra-diffusion equation was used to understand the resistance of the electrosorption process. The slope of this linear equation is the internal diffusion constant K_3. It can be seen from Figure 7 that as the concentration of the initial solution increases, the K_3 gradually increases. It is clearly indicated that the higher the concentration is, the greater intra-diffusion rate. The fitting degree of the straight line is very high, and the intercept of this line is roughly around zero, which indicates that the intra-diffusion step belongs to the rate control step in the electrosorption process and is closely related to the initial concentration.

At the same time, from the fitting results of the above quasi-first-order equation, it can be seen that the degree of fit is also very high, and the resistance of the electromigration step is also one of the main resistances of the electrosorption process. However, further analysis found that the value of the quasi-first-order dynamic constant does not correlate with the initial concentration, which indicates that the concentration of the initial solution does not affect the equilibrium solution concentration in the micropore because of the restriction of the intra-diffusion process.

The adsorption ions transfer process usually consists of three steps: the external diffusion step, the surface adsorption step and the internal diffusion step [20]. The second step, the surface adsorption step, is generally very rapid, so the resistance of this process can be ignored.

A key assumption implicit in the typical porous electrode CDI dynamic models is that the transmission resistance is ignored when the local ion transmission from macropores to micropores occurs, i.e., step 3 is ignored. This is correct when the pore size is large enough not to cause the electric double layer to overlap. Therefore, the main resistance of CDI desalination is simplified to the macroscopic transmission resistance, such as the CDI dynamic model based on the GCS double layer model established by Biesheuvel [21].

However, based on the experimental results obtained from Section 3, as well as the BJH diagram, we must additionally consider the influence of intra-diffusion resistance.

4. Establishment and Verification of the Electrosorption Dynamic Model

4.1. Dynamic Model Establishment

Initial CDI models utilized well known EDL structure models such as the Helmholtz or Gouy–Chapman–Stern (GCS) EDL models. However, neither of these models accurately captures the EDL structure along typical CDI electrodes' pore walls. For example, the GCS model established by Bazant assumes that the diffusion layer formed at the pore wall can extend freely [22]. However, in a typical multiscale CDI electrode, the pores with strong desalination have a small pore size (approximately less than 2 nm), so the EDL strongly overlaps [23].

In the m-D model mentioned above, the high overlap of the micropores is consistent with the actual situation, so we needed to use the modified Donnan theory to describe the electric double layer in this case. However, based on the results outlined in Section 3, we found that the chemical adsorption term μ_{att} can be ignored. Electrosorption is the main physical adsorption process for ACF electrode materials, so Equation (1) can be rewritten as follows:

$$c_{j,mi} = c_{j,mA} \times \exp(-Z_j \times \Delta\Phi_d) \tag{5}$$

The above equation is effective under the premise that ions are used as point charges in the average field approximation. The micropore volume charge density can be obtained by integrating the diffusion layer, σ_{mi} (mol·m^{-3}), where "mi" represents the micropores, and "mA" stands for macropores. In macropores, the concentrations of anions and cations are equal (locally neutrality), and only monovalent salt ion (1:1 type) solutions are considered in this system, so $c_{j,mA}$ can be used instead of the spacer channel salt concentration $c_{salt,mA}$, and it is also a function of time and position (depth) inside the electrode. The sum of the concentration equations of the two ions can directly give the total current density of all ions in the channel:

$$c_{mi} = c_{cation,mi} + c_{anion,mi} = 2c_{salt,mA} \times \cos h(\Delta\phi_d) \tag{6}$$

The micropore charge density σ_{mi} of local ions is derived from the anion and cation concentration equation as follows:

$$\sigma_{mi} = c_{cation,mi} - c_{anion,mi} = -2c_{salt,mA} \times \sin h(\Delta\phi_d) \tag{7}$$

In the equation, σ_{mi} is related to the potential difference $\Delta\varphi_{st}$ of the Stern layer:

$$\sigma_{mi}F = -C_{st,vol} \times \Delta\varphi_{st} \times V_T \tag{8}$$

$C_{st,vol}$ is the Stern layer capacitance per unit volume (F.m^{-3}), $V_T = RT/F$, R is the gas constant, T is the absolute temperature, and V_T is 25.7 mV at room temperature:

$$C_{st,vol} = C_{st,vol,0} + \alpha\sigma_{mi}^2 \tag{9}$$

Equation (9) is an empirical equation. Research by Biesheuvel [24] et al. showed that the capacitance of the Stern layer increases with the increase in the volume charge density in the micropores.

Due to the hypothesis that the cathode and anode electrode materials have equal mass, the salt adsorption capacity Γ_{salt} is a parameter to measure the adsorption performance of the electrode material, defined as the number of adsorbed ions per gram of electrode (the sum of two electrodes and excluding adsorption capacity when $V_{cell} = 0$), which can be expressed by σ_{mi} and $c_{ions,mi}$ as follows:

$$\Gamma_{salt} = \frac{1}{2}\frac{P_{mi}}{\rho} \times \left(c_{ions,mi} - c_{ions,mi}^0\right) \tag{10}$$

$$\Gamma_{salt} = \frac{P_{mi}}{\rho} c_{salt,mA} \cos h(\Delta\phi_d) - 1 \tag{11}$$

where P_{mi} is the micropore volume of the electrode per unit volume and ρ is the electrode material density. Note that $c^0_{ions,mi}$ subtracted from the above equation is the micropore concentration when the voltage is zero.

Anode and cathode balance charge "$\sum$" is:

$$\sum = \mp \frac{1}{2}\frac{P_{mi}}{\rho}\sigma_{mi} \tag{12}$$

The charge efficiency Λ is an important parameter that determines the performance of electrosorption desalination and energy consumption:

$$\Lambda = \frac{\Gamma_{salt}}{\sum} = -\frac{c_{ions,mi} - c^0_{ions,mi}}{\sigma_{mi}} = \tan h\left(\frac{\Delta\phi_d}{2}\right) \tag{13}$$

In the dynamic process, due to the spacer resistance and the electrode resistance, the potential drop between the spacer layer and the electrode is included in a potential drop $\Delta\phi_{tr}$. This potential drop is the main driving force across the electrode. The relationship between the potential drop everywhere and the external electric potential is:

$$\Delta V_{cell}/V_T = \Delta\phi_{tr} + 2|\Delta\phi_{st} + \Delta\phi_d| \tag{14}$$

In the equilibrium state of the adsorption process, where the driving force is equal to 0:

$$\frac{V_{cell}}{2V_T} = |\Delta\phi_d + \Delta\phi_{st}| \tag{15}$$

Among them, V_{cell} is the battery potential in V; F is the Faraday constant, 96,485 C/mol; $\Delta\phi_d$ and $\Delta\phi_{st}$ are the Donna potential and Stern potential, respectively, which are dimensionless units, and can be multiplied by V_T to get the potential in V.

According to the conservation of ion mass, the following identity can be obtained:

$$V_{tot} \times c_{salt,0} + V_{mi} \times c_{ions,mi,0} = V_{tot} \times c_{salt} + V_{mi}c_{salt,mi} = V_{mi} \times \varepsilon \tag{16}$$

Among them, V_{tot} is the volume of water in the entire system, including the circulation tanks, pipes, spacers, and macropores, but does not include the volume of water in the micropores; the subscript 0 refers to the initial concentration of the equation. The relationship between the ion charge density σ_{mi} in the micropores and the net charge density J is given by the following equation:

$$V_{mi}\frac{d\sigma_{mi}}{dt} = J \times A \tag{17}$$

Since J depends on the driving force of transportation (the unit is mol·m^{-2}·s^{-1}), A is the electrode area (m^2), and V_{mi} is the volume of micropores on the same sign electrodes (i.e., all anodes or all cathodes).

It is assumed that the salt concentration in the electrode macropore (the transmission path of the electrode) is consistent with the concentration in the spacer channel at each time. To describe the diffusion of ions in the spacer layer and the electrode, the net current density J, a single relationship between the voltage drop $\Delta\phi_{tr}$ and the salt concentration c can be used to obtain the current density J:

$$J = J_{Na} - J_{cl} = k \cdot c_{i,mA} \times \Delta\phi_{tr} \tag{18}$$

Among them, k is the transfer coefficient (in m.s^{-1}), which is a function of the effective ion diffusion coefficient and the resistance of the spacer and the electrode:

$$J = k \times \left(\frac{V_{cell}}{V_T} + 2\frac{\sigma_{mi} \times F}{C_{st,vol}} + 2 \times \frac{asinh\sigma_{mi}}{2c_{i,mA}} \right) \tag{19}$$

The micropore ions concentration is obtained by combining Equations (5) and (6) which leads to:

$$c_{mi} = \sqrt{\sigma_{mi}{}^2 + 4c^2} \tag{20}$$

Combined with the Equation (15), we can finally determine the expression of the spacer concentration:

$$c = \frac{\sqrt{b^2 - 4 \cdot \beta\left(\sigma_{mi}^2 - \varepsilon^2\right)} - b}{2 \times \beta}, \beta = -\left(\frac{v_{tot}}{v_{mi}}\right)^2, b = 2\varepsilon\frac{v_{tot}}{P_{mi}} \tag{21}$$

4.2. Model Fitting Analysis and Verification

The mass of two electrodes is 40 g, the micropore volume V_{mi} is 10.14 mL, V_{tot} is 489.86 ml, the electrode geometrical area A is 0.1 m^2 and p_{mi} is 0.2028. From the fitting of the m-D model to the equilibrium data, we obtained parameter estimates for $C_{st,vol,0}$, α. Fitting to the time-dependent part of the data, the only remaining parameter is the transfer coefficient k to fit all possible data points.

The actual desalination capacity of the ACF electrosorption device was compared with the desalination capacity simulated by the above model, as shown in Figure 9. The point in the figure represents the change of the actual desalination capacity over time, and the fitting line represents the adsorption capacity based on the theoretical model. It can be seen in the figure that the model we selected can fit the actual desalination data well, indicating that the simplified dynamic CDI model is effective for this electrosorption process.
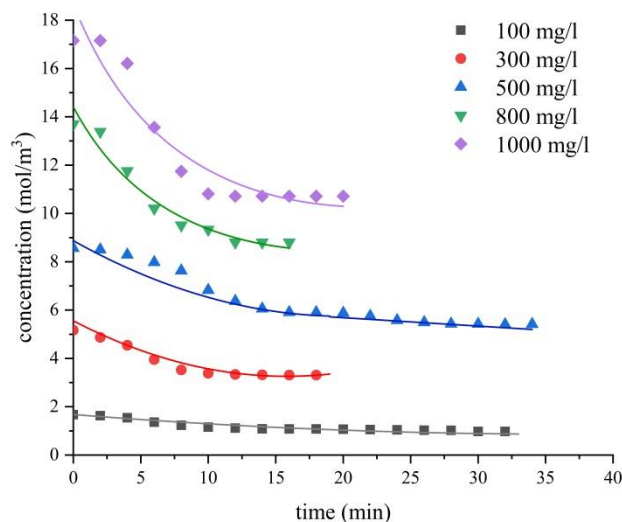
Figure 9. Salt concentration vs. time in batch-mode CDI experiment. Lines: theory; dots: experimental data.

However, the effective microporous porosity p_{mi} (the effective micropore volume relative to the total electrode volume) is not a fixed value for the same material under all working conditions. The above fitting results were obtained by using the definite value of p_{mi} which was calculated by the characterization results. For example, as the initial concentration increases, the cut-off pore size decreases, and the corresponding effective micropore porosity increases; as the voltage increases, p_{mi} should also increase continuously without

exceeding the electrolysis voltage of water. In future work, the quantitative influence of voltage and concentration on p_{mi} can be discussed to improve the reliability of the model.

5. Discussions

With the development of improved electric double layer structure models, it is also important that the electric double layer structure model must be simple enough to be easily integrated into the porous electrode transport model. When the models are extended to typical ion mixing situations in actual environmental applications, they should remain mathematically concise. From the perspective of development, several models are getting closer and closer to objective facts, and there is no perfect model. The proposal of more updated electric double layer models is the cornerstone of the future development of the field of interface dynamics.

The ultimate goal of electrosorption modeling is to derive a mathematical equation that can not only describe the previously recorded data but also predict the performance of CDI in various aspects, including the degree of desalination, pH fluctuations, and energy consumption. This model should be able to be implemented in a wide range of input parameters (thickness, porosity) of the electrode structure, battery design, and external conditions (such as switching time, applied current, and voltage signals) [25]. At the same time, the future model can be combined with a cost calculation module that includes energy and material prices together with a cost optimization equation to calculate the best CDI system design and operation condition. This goal is still far from being achieved.

6. Conclusions

(1) Quasi-first-order and quasi-second-order dynamic equations were used to fit the curve of the ACF electrosorption adsorption capacity with time under different concentrations. We found that the electrosorption process is mainly physical adsorption, almost without Redox reaction presence related to the Faraday capacitor. As the concentration increases, the quasi-first-order rate constant gradually increases. It can be seen that the greater the concentration of the injection solution, the greater the electrosorption rate.

(2) The intra-diffusion equation was used to study the ion transfer resistance. The intra-diffusion step is one of the control steps of the electrosorption process through the analysis of the fitting curve. In the dynamic modeling process, the total resistance cannot be simply described as the macroscopic transmission resistance across the electrode.

(3) Under the condition of accurately considering the dynamic mechanism of electrosorption, the electrosorption dynamic model in the batch mode method was obtained based on the macroscopic porous electrode theory and the modified Donnan model theory. The feasibility and accuracy of the model were verified by fitting experimental data.

Author Contributions: Conceptualization, S.M.; data curation, L.H.; formal analysis, L.M.; investigation, L.M.; methodology, L.M.; resources, Y.X. and F.W.; software, L.H. and C.L.; supervision, S.M.; writing—review and editing, C.L., H.X. and S.M. All authors have read and agreed to the published version of the manuscript.

Informed Consent Statement: Informed consent was obtained from all subjects involved in the study.

Data Availability Statement: The data presented in the study are available on request from the corresponding author.

Conflicts of Interest: The authors declare no conflict of interest.

References

1. Zhao, R.; van Soestbergen, M.; Rijnaarts, H.H.; van der Wal, A.; Bazant, M.Z.; Biesheuvel, P.M. Time-dependent ion selectivity in capacitive charging of porous electrodes. *J. Colloid Interface Sci.* **2012**, *384*, 38–44. [CrossRef] [PubMed]

2. Hasseler, T.D.; Ramachandran, A.; Tarpeh, W.A.; Stadermann, M.; Santiago, J.G. Process design tools and techno-economic analysis for capacitive deionization. *Water Res.* **2020**, *183*, 116034. [CrossRef] [PubMed]

3. Raluy, R.G.; Schwantes, R.; Subiela, V.J.; Peate, B.; Betancort, J.R.J.D. Operational experience of a solar membrane distillation demonstration plant in Pozo Izquierdo-Gran Canaria Island (Spain). *Desalination* **2012**, *290*, 1–13. [CrossRef]

4. Li, H.; Zou, L.J.D. Ion-exchange membrane capacitive deionization: A new strategy for brackish water desalination. *Desalination* **2011**, *275*, 62–66. [CrossRef]

5. Lee, H.J.; Sarfert, F.; Strathmann, H.; Moon, S.H. Designing of an Electrodialysis desalination plant. *Desalination* **2002**, *142*, 267–286.

6. Greenlee, L.F.; Lawler, D.F.; Freeman, B.D.; Marrot, B.; Moulin, P.J.W.R. Reverse osmosis desalination: Water sources, technology, and today's challenges. *Water Res.* **2009**, *43*, 2317–2348. [CrossRef]

7. Chen, Z.; Song, C.; Sun, X.; Guo, H.; Zhu, G.J.D. Kinetic and isotherm studies on the electrosorption of NaCl from aqueous solutions by activated carbon electrodes. *Desalination* **2011**, *267*, 239–243. [CrossRef]

8. Arnold, B.B.; Murphy, G.W. Studies on the electrochemistry of carbon and chemically-modified carbon surfaces. *J. Phys. Chem.* **1961**, *65*, 135–138. [CrossRef]

9. Chang, L.M.; Duan, X.Y.; Liu, W.J.D. Preparation and electrosorption desalination performance of activated carbon electrode with titania. *Desalination* **2011**, *270*, 285–290. [CrossRef]

10. Lim, J.A.; Park, N.S.; Park, J.S.; Choi, J.H.J.D. Fabrication and characterization of a porous carbon electrode for desalination of brackish water. *Desalination* **2009**, *238*, 37–42. [CrossRef]

11. Wang, W.; Zhang, S.; Chinwangso, P.; Advincula, R.C.; Lee, T.R. Electric Potential Stability and Ionic Permeability of SAMs on Gold Derived from Bidentate and Tridentate Chelating Alkanethiols. *J. Phys. Chem. C* **2014**, *113*, 3717–3725. [CrossRef]

12. Park, K.K.; Lee, J.B.; Park, P.Y.; Yoon, S.W.; Moon, J.S.; Eum, H.M.; Lee, C.W. Development of a carbon sheet electrode for electrosorption desalination. *Desalination* **2007**, *206*, 86–91. [CrossRef]

13. Kinraide, T.B. Use of a Gouy-Chapman-Stern model for membrane-surface electrical potential to interpret some features of mineral rhizotoxicity. *Plant Physiol.* **1994**, *106*, 1583–1592. [CrossRef]

14. Mizuno, Y.; Okubo, M.; Asakura, D.; Saito, T.; Hosono, E.; Saito, Y.; Oh-Ishi, K.; Kudo, T.; Zhou, H. Impedance spectroscopic study on interfacial ion transfers in cyanide-bridged coordination polymer electrode with organic electrolyte. *Electrochim. Acta* **2012**, *63*, 139–145. [CrossRef]

15. Yang, K.-L.; Ying, T.-Y.; Yiacoumi, S.; Tsouris, C.; Vittoratos, E.S. Electrosorption of ions from aqueous solutions by carbon aerogel: An electrical double-layer model. *Langmuir* **2001**, *17*, 1961–1969. [CrossRef]

16. Porada, S.; Zhao, R.; van der Wal, A.; Presser, V.; Biesheuvel, P.M. Review on the science and technology of water desalination by capacitive deionization. *Prog. Mater. Sci.* **2013**, *58*, 1388–1442. [CrossRef]

17. Biesheuvel, P.M.; Porada, S.; Levi, M. Attractive forces in microporous carbon electrodes for capacitive deionization. *J. Solid State Electrochem.* **2014**, *18*, 1365–1376. [CrossRef]

18. Nordstrand, J.; Laxman, K.; Myint, M.T.Z.; Dutta, J. An Easy-to-Use Tool for Modeling the Dynamics of Capacitive Deionization. *J. Phys. Chem. A* **2019**, *123*, 6628–6634. [CrossRef]

19. Dykstra, J.E.; Dijkstra, J.; van der Wal, A.; Hamelers, H.V.M.; Porada, S. On-line method to study dynamics of ion adsorption from mixtures of salts in capacitive deionization. *Desalination* **2016**, *390*, 47–52. [CrossRef]

20. Fulazzaky, M.A. Determining the resistance of mass transfer for adsorption of the surfactants onto granular activated carbons from hydrodynamic column. *Chem. Eng. J.* **2011**, *166*, 832–840. [CrossRef]

21. Biesheuvel, P.M.; Bazant, M.Z. Nonlinear dynamics of capacitive charging and desalination by porous electrodes. *Phys. Rev. E* **2010**, *81*, 031502. [CrossRef] [PubMed]

22. Bazant, M.Z.; Thornton, K.; Ajdari, A. Diffuse-charge dynamics in electrochemical systems. *Phys. Rev. E* **2004**, *70*, 021506. [CrossRef] [PubMed]

23. Porada, S.; Bryjak, M.; van der Wal, A.; Biesheuvel, P.M. Effect of electrode thickness variation on operation of capacitive deionization. *Electrochim. Acta* **2012**, *75*, 148–156. [CrossRef]

24. Shocron, A.N.; Suss, M.E. The effect of surface transport on water desalination by porous electrodes undergoing capacitive charging. *J. Phys.* **2017**, *29*, 084003. [CrossRef] [PubMed]

25. Suss, M.E.; Porada, S.; Sun, X.; Biesheuvel, P.M.; Yoon, J.; Presser, V. Water desalination via capacitive deionization: What is it and what can we expect from it? *Energy Environ. Sci.* **2015**, *8*, 2296–2319. [CrossRef]